

RESEARCH ARTICLE

NMR study of nitrate ionic liquids confined between micrometer-spaced plates

Andrei Filippov^{1,*}, Oleg I Gnezdilov², Maiia Rudakova¹, Rustam Gimatdinov³, Victor P. Arkhipov⁴,
Oleg N. Antzutkin¹

¹ *Chemistry of Interfaces, Luleå University of Technology, SE-97187 Luleå, Sweden*

² *Institute of Physics, Kazan Federal University, 420008 Kazan, Russia*

³ *Medical and Biological Physics, Kazan State Medical University, 420012, Kazan, Russia*

⁴ *Department of Physics, Kazan National Research Technological University, 420015, Kazan, Russian Federation*

* **Corresponding author:** Andrei Filippov, andrei.filippov@ltu.se

ABSTRACT

This review paper presents the results of a study conducted using nuclear magnetic resonance (NMR) methods to investigate the dynamic behaviour of ionic liquid-based compositions in micrometre-spaced confinement. Ethylammonium nitrate (EAN) and other ionic liquid (IL) systems with nitrate anion in glass or quartz spaced confinement demonstrate anomalous cation dynamics that differ from those observed in bulk and in nano-confinement. It was demonstrated that the principal axis of the nitrate anion exhibits preferential orientation to the surface, akin to that in liquid crystals. It was shown that the cation translational mobility reversibly changes during exposure to a static magnetic field. This phenomenon was interpreted as a result of intermolecular structure transformations occurring in the confined ILs. The mechanisms of these transformations were discussed.

Keywords: diffusivity; ion dynamics; phase transformation; confined ionic liquid

ARTICLE INFO

Received: 26 March 2024

Accepted: 8 May 2024

Available online: 15 May 2024

COPYRIGHT

Copyright © 2024 by author(s).

Applied Chemical Engineering is published by Arts and Science Press Pte. Ltd. This work is licensed under the Creative Commons Attribution-NonCommercial 4.0 International License (CC BY 4.0).

<https://creativecommons.org/licenses/by/4.0/>

1. Ionic liquid in interfaces and in nano-confinements

Ionic liquids (ILs) are ionic compounds formed typically of organic cations and either organic or inorganic anions. These compounds remain in the liquid state at temperatures below 100 °C, which has led to their attraction as solvents for the replacement of organic liquids in “green” chemical synthesis, as components of lubricants, and as electrolytes for electrochemical devices. Due to the multitude of interactions inherent to ILs in bulk (Coulombic, van der Waals, hydrogen bonding, etc.), numerous ILs exhibit ordering of ions and form well-defined nanostructures with regions of polar and nonpolar domains^[1-6]. The growing application of ILs has led to the challenge of understanding the properties of ILs near surfaces^[7-10] and in confining geometries^[1,11,12-23]. It is well established that the structure and properties of molecular liquids in these conditions are significantly different from those in bulk. These properties are affected by size, shape, and topology of geometric restrictions, which influence rates of chemical reactions, electrical conductivity, thermal properties, and viscosity.

Studies of protic (PILs) and aprotic (AILs) in contact with air and solid surfaces revealed different molecular structures of ILs^[22] by Atomic Force Microscopy (AFM) and computer simulations. The solid surfaces were composed of carbon in the form of graphite and graphene^[22], mica^[10,24], silica^[8,14,24] and metals^[9]. It has been demonstrated that the most prevalent structure formed by ILs in proximity to the surface is a layered structure. These structures comprise alternating layers of cations and anions. Additionally, the preferential orientation of ions near the surface was mentioned. The charge of these layers is dependent on the properties of the surface. The layered structure has been observed to extend up to a few nanometers^[3,7,24]. There have been multiple studies that have focused on IL structure near the surface^[10,24] and between micrometer-spaced solid surfaces^[25,26]. The structure and extension of layers were studied in terms of the influence of surface charge and roughness^[24]. The long-range ordering of imidazolium ILs between slowly rotating disks was demonstrated using a combination of FTIR, Ellipsometry, and Secondary-Harmonic Generation methods^[25]. Smectic mesophase was found by SAXS/WAXS methods in octadecylimidazolium ILs confined between plates separated by 4 μm . It was mentioned that the application of a magnetic field affects the mesophase mosaicity^[26].

Most publications about IL-confined systems focused on nanoporous, microporous, and mesoporous materials, while macroporous systems received less attention. Carbon and silica are two commonly used materials. The behavior of confined ILs is a combination of a 'surface contribution' and a 'bulk-like contribution' caused by ions located in the pore center^[17,21]. Depending on the molecular details of the confining space and the type of IL, the diffusivities of confined ILs may increase^[1,15,16,27,28] or decrease^[1,14,22]. The conductivity of confined ILs was comparable to or even higher than the bulk ionic conductivity^[29]. The layered structure over a few nanometers from the pore wall has been observed^[17,21], and the formation of this structure is driven by electrostatic interactions^[21]. The melting temperature of nanoporous-confined ILs decreases according to the Gibbs-Thomson equation^[11].

2. Properties of bulk, near surfaces and in nano-confinement nitrate ILs

Ethylammonium nitrate (EAN) and propylammonium nitrate (PAN) (**Figure 1**) are the most extensively studied protic ILs^[30-32]. EAN is employed as a reaction medium, precipitating agent^[33], and electrolyte for supercapacitors^[34,35]. PAN has potential applications in self-assembly media, catalysts, and biological agents^[36]. The bulk structures of EAN and PAN were investigated, and nanoscale heterogeneity connected to the smectic phase was found^[37,38]. Neutron diffraction demonstrated that bulk EAN has a long-range structure with a domain size of one nm^[6]. The structure is similar to a bicontinuous microemulsion or disordered L_3 -sponge phase. On the other hand, 1-ethyl-3-methyl-imidazolium nitrate is aprotic IL.

The T_1 relaxation recovery for ^1H of different groups demonstrates forms close to the exponential ones. The T_2 relaxation for the $-\text{NH}_3$ group was exponential while for of $-\text{CH}_2-$ and $-\text{CH}_3$ groups (**Figure 2**) it was close to the sum of the two-exponential^[12].

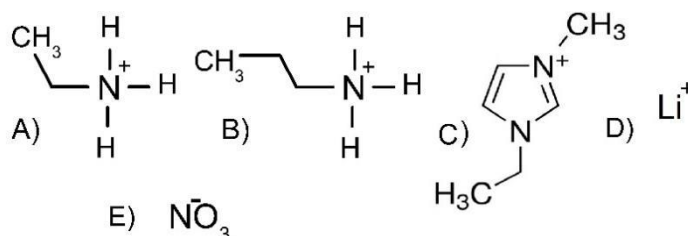


Figure 1. Chemical structures of ILs ions: A) ethylammonium (EA) cation; B) propylammonium cation; C) 1-ethyl-3-methyl-imidazolium cation, D) Li⁺ ion, and E) nitrate anion.

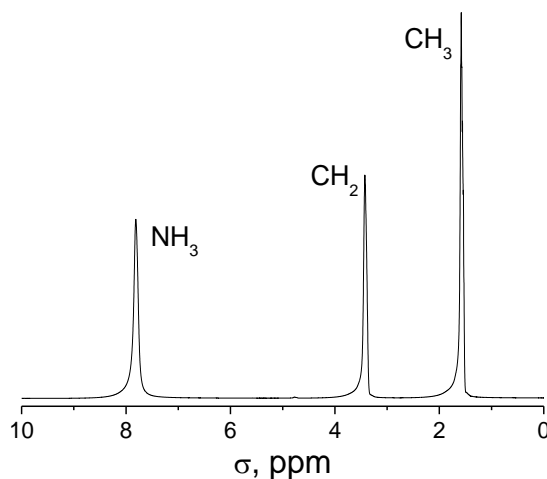


Figure 2. ^1H NMR spectrum of EAN in CDCl_3 . $T = 303 \text{ K}$ ^[12].

The resonance lines assigned to the NH_3^+ (7.63 ppm), CH_2 (3.21 ppm) and CH_3 (1.36 ppm) EA cation.

Mean T_2 times were essentially less than T_1 for all chemical groups of EA (**Figure 3**). This is a typical for viscous liquids, where the primary relaxation mechanism for ^1H relaxation is dipolar coupling^[39], and the reorientation correlation time is expressed like $\tau_c \gg 1/\omega_0$.

Diffusion decays (DDs) for EA cations on ^1H and for nitrate anions on ^{15}N isotopes were obtained by the PFG NMR method. All DDs were one-exponential form and didn't depend on the diffusion time^[12]. In the temperature range of 293-363 K, the anions diffusion coefficient (DC) was found to be approximately 1.7 times greater than that of the EA cations. (**Figure 4**).

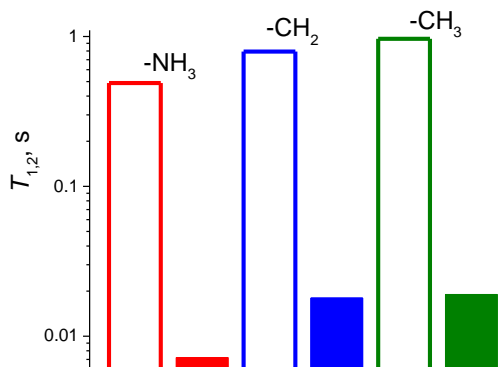


Figure 3. ^1H NMR T_1 (open) and T_2 (filled) relaxation times of bulk EAN [17]. $T=293 \text{ K}$.

Temperature dependence of the DC of EA was analysed in the 283-363 K temperature range^[40] and was described by the Vogel-Fulcher-Tammann (VFT) equation:

$$D = D_0 \exp\left(\frac{-E_D}{R \cdot (T - T_0)}\right) \quad (1)$$

where D_0 , T_0 and E_D are adjustable parameters. Non-Arrhenius dependences are typical for ILs^[40-42]. T_0 indicates so-called “dynamic glass transition temperature”^[43].

In the case of EAN (**Figure 4**) Arrhenius equation can be applied:

$$D = D_0 \cdot \exp(-E_D/RT), \quad (2)$$

which gives the apparent activation energy for anions and cations diffusion $E_D \sim 4 \text{ kJ/mol}$ ^[40].

A remarkable result concerning the peculiarities of diffusion in bulk ILs is the difference in DCs of almost twice between EA cations and NO_3^- -anions^[12]. It is assumed that in a free ILs, cations and anions are in the

paired state most of the time, which implies close values of DCs. It is also known that the studied cations and anions have comparable sizes^[10,24,44], which should lead to approximately equal values of DCs if we assume that ions can move independently in the IL. The observed difference in the ionic mobility of cations and anions can be explained by the presence of the heterogeneous nanoscale structure^[4,6]. The source of such self-organization in bulk ILs is the association of EA cations due to their solvophobicity^[4,6].

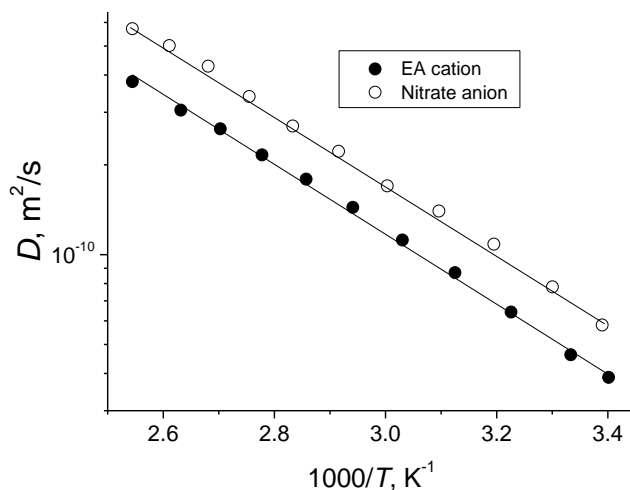


Figure 4. Arrhenius plot of the temperature dependences of DCs of the EA cations and the NO₃⁻ anions obtained by PFG NMR on ¹H and ¹⁵N nucleus, respectively^[12].

Nanoconfinement nitrate ILs like EAN and PAN were investigated in the last few years^[3,12,17-19,24]. For example, it has been shown by AFM that the EAN confined between mica plates exhibits electrostatic interaction with the substrate surface at a distance of more than two nm and the formation of a layered ionic liquid structure near the mica surface^[24]. Furthermore, NMR data indicated that the polytetrafluoroethylene (PTFE) surface induces a low diffusivity EAN region in its vicinity^[19]. Additionally, efforts have been made to investigate the behavior of ionic liquids confined within porous media through the use of NMR and molecular dynamic simulations^[17,19,45]. According to some estimates, the pore surface exerts a significant influence on the ionic liquid dynamics only in a very small region of approximately 1-2 nm^[17]. Diffusion of EAN confined within pores of two types of porous glass, Vycor® and Varapor, with average pore sizes of 4 nm and 9.8 nm, respectively, was studied by ¹H NMR in the temperature range of 295-325 K^[45]. It was shown that the diffusional behavior of the EA cation corresponds to long-term diffusion in a system of interconnected pores. Diffusivity of the IL in Varapor is controlled by the porous system's tortuosity and does need to take into consideration the interaction with the surface of the discrete pore walls. In the case of Vycor®, the long-term diffusivity is a factor 1.5 lower than that expected in the absence of interaction with the pore walls. Two possible mechanisms were suggested that may explain this discrepancy: the EAN-surface interaction and the retardation of EAN diffusion in smaller pores present in Vycor® porous glass due to pore size distribution^[45].

3. Diffusivity and NMR relaxation of the micrometer-spaced confined nitrate ionic liquids

3.1. Diffusivity and NMR relaxation

The stack of glass plates with IL (**Figure 5**) spaced by 3.8-4.5 μm was placed in the NMR solenoid ¹H insert for diffusivity and NMR relaxation measurements^[12]. This type of samples has an axis that is normal to the surface of the stack plates. This feature allows for sample orientation at different angles to the SMF direction^[12].

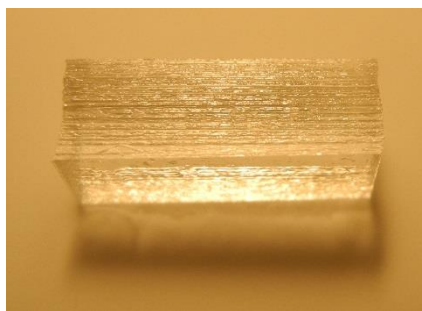


Figure 5. The stack of glass plates with confined of EAN^[12].

The values of T_1 and T_2 of EA confined between glass plates were found to differ from those in bulk (**Figure 6**). The T_1 of protons of all groups of EA and the T_2 of the $-\text{CH}_2-$ and $-\text{CH}_3$ groups of EA exhibited a change of 5-10%^[18]. The reliable change occurred with the T_2 of the $-\text{NH}_3$ protons, which decreased by a factor of ~ 22 relative to their bulk values^[12]. Diffusion measurements were conducted in two directions. For both orientations, the DDs were in the exponential form. The parallel DC was independent of the diffusion time, whereas the normal DCs were dependent on the diffusion times, as a result of the restricted planar geometry of the glass plates^[12,46]. The DCs were found to be higher than that in the bulk by a factor of 2–3 (**Figure 6**)^[12]. The analysis^[12,18] allowed the authors to conclude that the observed alterations in the NMR relaxation rates of the EA protons and the enhancement of the diffusion of the EA cation as a whole are not artefacts but are the result of an entirely molecular structural effect.

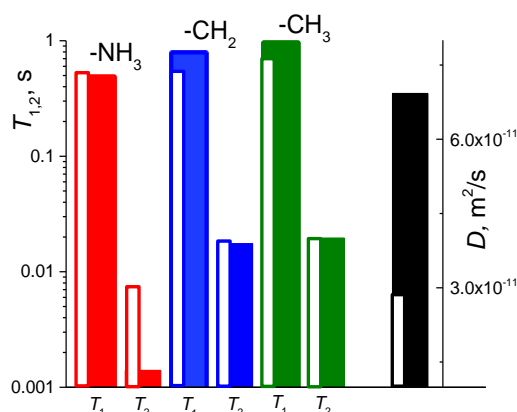


Figure 6. ^1H NMR T_1 and T_2 relaxation times for EA groups: bulk - coloured open bars and confined - coloured filled bars. EA diffusion coefficients for bulk - open black bars and for confined - filled black bars^[12]. $T = 293$ K.

3.2. NMR diffusion and relaxation of confined ILs exposed in the SMF

For EAN layers confined between glass plates and placed in a strong static magnetic field (SMF), values of T_1 , T_2 , and DC of the EA cations were observed to depend on time (**Figure 6**)^[18]. Similar effects were reported for other protic ILs^[47].

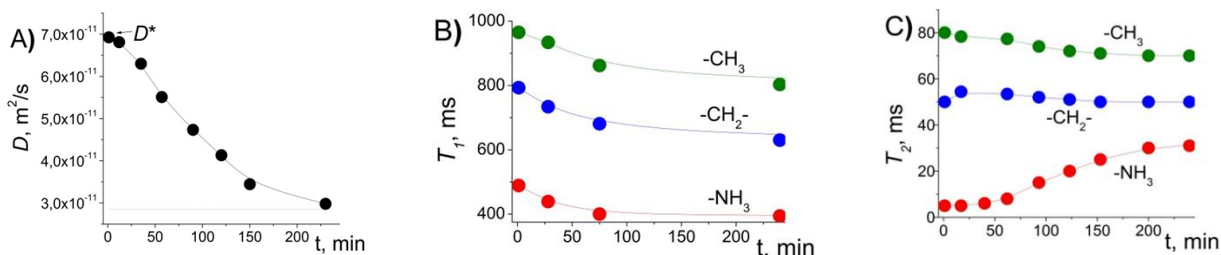


Figure 6(A, B, C). T_1 NMR relaxation times and C) T_2 NMR relaxation times of protons of EA cations chemical groups for EAN confined at 9.4 T SMF^[18]. DC was measured parallel to the plates, $t_d = 3$ ms.

For [EMIm][NO₃]IL, the diffusivity is also increased after confinement between plates and gradually decreases under the influence of SMF (**Figure 7A**)^[47]. For bulk solutions of LiNO₃ in EAN, 1.9-15 wt%, the diffusivities of the Li⁺ ions are lower than the diffusivity of the EA cations^[42] (**Figure 7B**). Therefore, the effects of increased diffusivity of cations of ILs neat and in mixed systems with nitrate ions are common for protic and aprotic ILs and metal ions such as Li⁺. Further studies were conducted to examine the influence of various conditions on the observed effects in the case of EAN^[40,48-51].

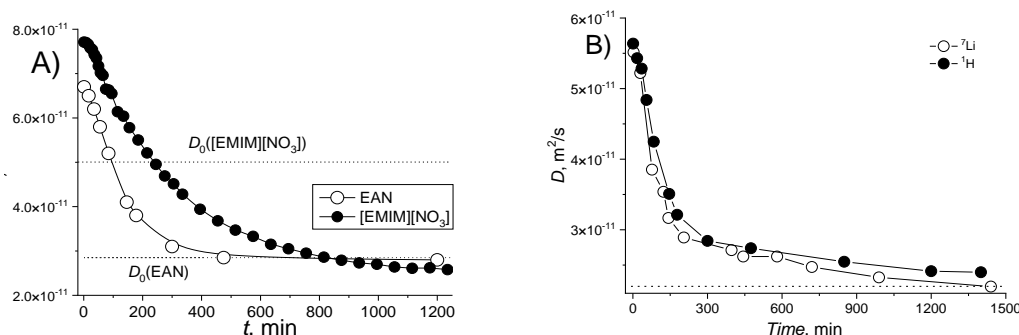


Figure 7A. DCs of the EA cations and [EMIm]⁺ B) DCs of EA cations and Li⁺ in a mixture 15 mol% of LiNO₃ glass plates confined ILs at SMF^[42,47]. D was measured along the plates, t_d = 3 ms. Dotted lines show DCs of bulk ILs.

3.3. Effects in IL/water solutions

¹H NMR diffusometry experiments were performed on mixtures of EAN-water (3.1-12.4 mol%) confined between polar glass plates and exposed to SMF^[49]. The diffusion of both EAN and water is single component and no diffusion time dependence of the DCs was found in the range of diffusion times 3 - 300 ms. In bulk EAN-water mixtures, increasing the water content leads to an increase in both DCs and the DCs don't change with SMF exposure^[12]. On the other hand, the diffusion behavior of EAN-water mixtures confined between plates appears quite unusual. The placement of EAN-water mixtures in SMF leads to an increase in EAN DC for samples with a water content of 0-6.2 mol% that is larger than the bulk EAN DC (**Figure 9**). However, the ratio of the EAN DC to bulk EAN DC decreased from 3.8 to 1.4, respectively. For mixtures with 12.4 mol% of water, EAN DC is less than bulk EAN DC. The DCs for water are larger for a sample with 3.1 mol% and smaller for samples with 6.2 and 12.4 mol% of water than the bulk values for water DCs.

It was proposed that the bulk EAN-water structure^[52] could undergo a change due to interactions with the polar glass surface, in accordance with the phase diagram of the EAN-water mixture^[52]. Furthermore, it was suggested that unusual diffusion could be conditioned by a phase transformations in the EAN-water system. As the exposure time increased, the diffusivity of EAN decreased and the DC of EAN reached a stationary value, D_∞. This D_∞ value is comparable to the confined neat EAN DC (**Figure 9**), yet this EAN-water system state differs from the previously described bulk or confined states. It appears that EAN exists in two distinct liquid phases: one comprising an EAN-water mixture, and another comprising neat EAN^[49]. The ¹H NMR water signal exhibited a decrease with increasing exposure time, with complete disappearance observed at approximately 200 minutes for the 3.1 mol% sample, 600 minutes for the 6.2 mol% sample, and 100 minutes for the 12.4 mol% sample, respectively (**Figure 9**). It is possible that water exists in two physical states. The first type is characterised by NMR relaxation times typical of liquids, which led to the measurement of NMR diffusivity. The second type is characterised by “solid-like” NMR relaxation features that make it “invisible” to the NMR diffusometry technique. It was proposed that this second type corresponds to adsorbed water on the glass plates^[52].

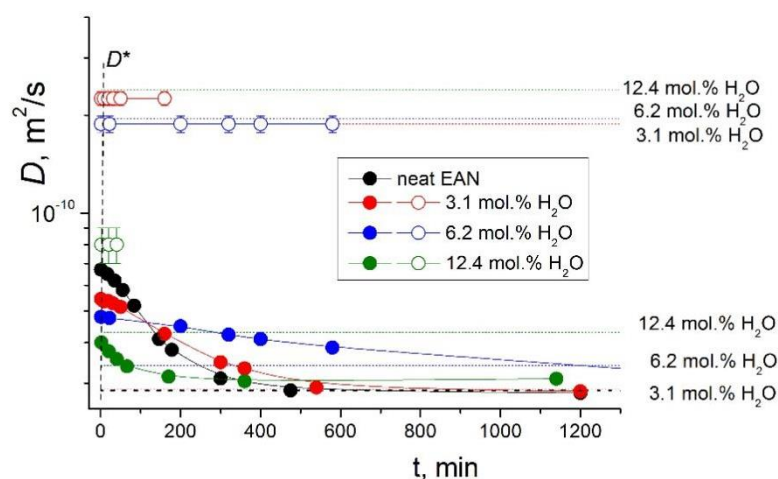


Figure 8. DCs of EAN-H₂O mixtures at different exposure times to SMF^[49]. Black dotted line corresponds to EAN, coloured dotted lines correspond to bulk mixtures, and symbols and solid lines correspond to confined systems: EAN (solid circles) and water (open circles). D*s are EAN and water DCs after placement in SMF.

3.4. Effect of surface roughness

The NMR data for EAN and EAN-water confined systems that drive by the chemical composition of plates does not exhibit a significant difference. Borosilicate glass plates and fused quartz glass plates were used for the experiments^[47].

The surface roughness and surface area of the glass plate may influence the dynamic behaviour of confined ILs^[48]. To elucidate the impact of these characteristics, glass plates treated with hydrofluoric (HF) acid aqueous solutions were subjected to investigation. The BET method^[53] was employed to analyse both untreated and HF-treated glass plates. The BET surface area was found to be 0.1 ± 0.01 m²/g for the untreated glass plates and 0.05 ± 0.01 m²/g for the HF-treated glass plates. **Figures 9A and 9B** present atomic force microscopy (AFM) images of glass plate surfaces before and after the HF-treatment, respectively. The untreated surface is relatively flat, with height variations of no more than 1 nm. In contrast, the HF-treated glass surface exhibits height variations of up to 400 nm. Consequently, the surface area of micropores is reduced, while that of macropores (greater than 50 nm) is increased, as observed in^[48].

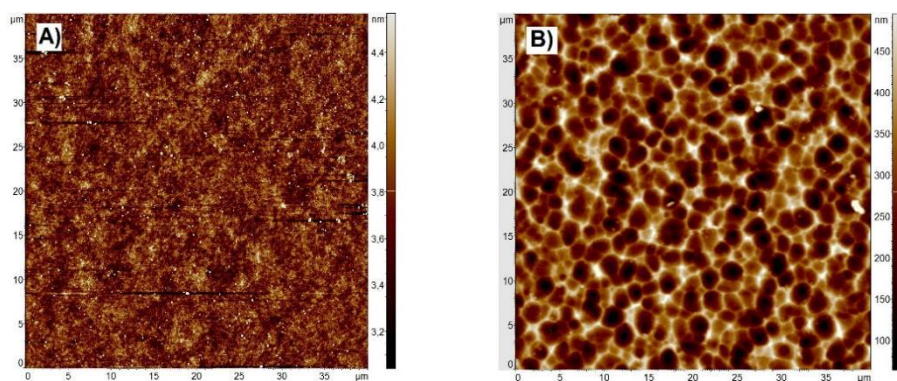


Figure 9. Atomic force microscopy images of untreated (A) and HF-treated (B) surfaces of glass plates^[48].

The results of ¹H NMR diffusion experiments on HF-treated glass plates confined EAN demonstrated a similar phenomenon to that observed for untreated plates. The DC was approximately 12% higher than that observed for EAN confined by untreated glass plates. The exposure of untreated glass plates to SMF resulted in a decrease in the DC of EA cations over time. It was postulated that the observed difference is correlated with the fraction of small pores in untreated and HF-treated glass plates and is related to the dominance of surface properties contributions in the micrometer-scale range.

The distance between the glass plates was found to exhibit small variations when comparing results obtained on untreated glass plates^[12,18] with those obtained on vacuum-deposited TiO₂ on the edges of the plates^[48], with a distance between the plates of 3-4.5 μm. The observed effects in the EAN systems and the rate of DC decrease of the EA cations are comparable for both types of samples^[48].

3.5. Effects of temperature

In further discussion the term “phase” for EAN in bulk state, confined between glass plates and confined between glass plates and exposed to SMF as I_B, I and I_{MF}, respectively was used. Dependences of ¹H NMR chemical shift and DCs of EA cations were analysed in the temperature range of 293-363 K. It was found that NMR chemical shift of NH₃ protons in the I phase was strongly shifted upfield (**Figure 10**) because of weakening of the hydrogen-bonding network of the confined EAN^[40].

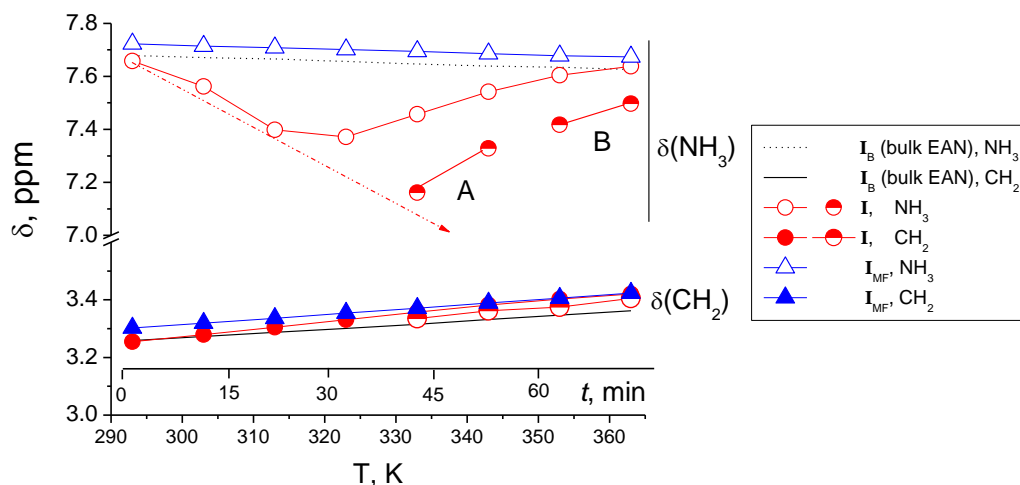


Figure 10. Temperature dependences of ¹H NMR chemical shifts of bulk EAN chemical groups, EAN glass plates confined in the I_{MF} phase and EAN experiencing I → I_{MF} transition^[40]. Axis t shows the experiments time. Temperatures are 333 K(A) and 353 K (B).

The temperature dependences of DCs follows the order D(I) > D(I_B) > D(I_{MF}) (**Figure 11**) and describes by VFT equation (Eq.3).

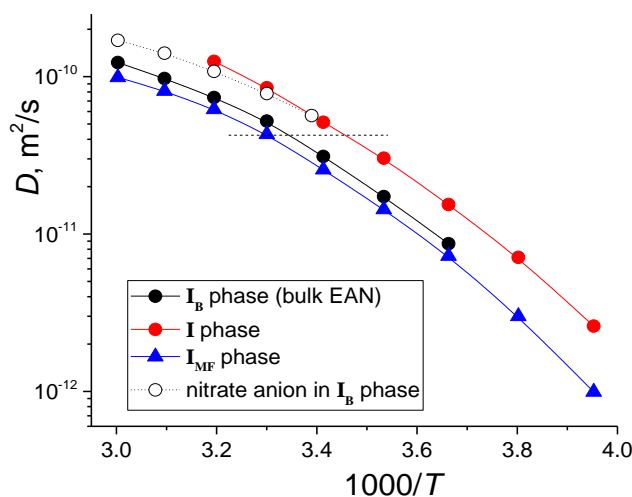


Figure 11. Temperature dependences of DCs of the EA cations in I_B phase, (black circles), in I phase (red circles), in I_{MF} phase (blue triangles)^[40] and of [NO₃]⁻ anions in I_B phase^[12]. Lines show best fits with the VFT equation.

Based on estimated apparent activation energies of EA cations it was assumed that transitions I_B→I is an endothermic process and I→I_{MF} and I_{MF}→I are exothermic and endothermic for confined EAN.

The temperature dependencies of ^1H NMR spectra integral intensities of EAN in I and I_{MF} phases at cooling and heating^[51] were investigated at the range 293-256 K (**Figure 12**). These dependencies have different forms, but for both of one's demonstrate an abrupt decrease. The decrease of the signal occurs for I phase at ~ 263 K, and for I_{MF} phase at ~ 266 K at cooling (**Figure 12A**). These temperatures are much lower than EAN in I_{B} phase (~ 285 K)^[54]. For I_{MF} the signal completely disappeared at temperatures below 266 K (**Figure 12A**). However, for the I phase the typical ^1H NMR spectra of EAN with an integral amplitude of ~ 0.24 was maintained down to 256 K. For the heating cycle (**Figure 12B**) the melting of the I_{MF} phase occurred sharply at 289 K. For the I phase, the process of melting began at temperature 270 K, and “smeared” over the temperature range up to ~ 285 K.

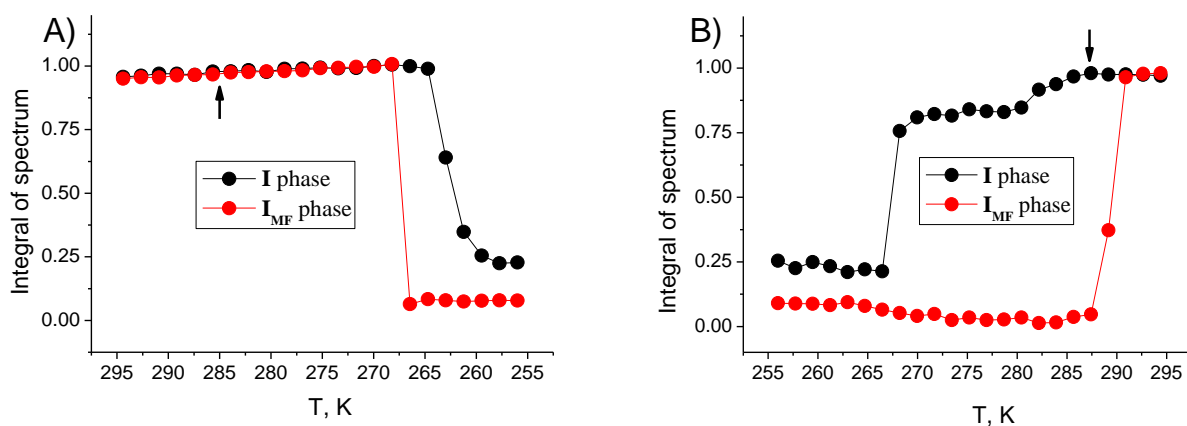


Figure 12. Temperature dependencies of ^1H NMR spectra integral intensities of EAN in I and I_{MF} phases at A) cooling and B) heating^[51]. Arrows show the melting temperature of EAN in I_{B} phase.

^1H NMR spectra obtained for phases I and I_{MF} at heating are shown in **Figure 13**.

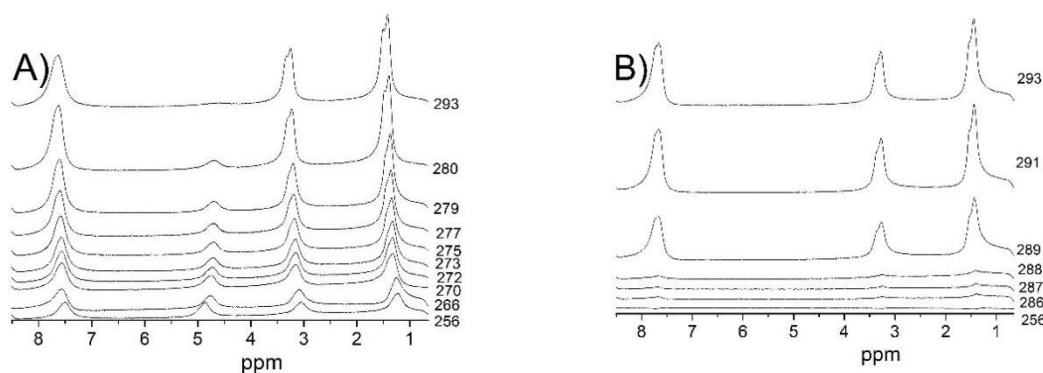


Figure 13. ^1H NMR spectra dependencies of EAN polar glass plates confined from the temperature 256-293 K: A) before and B) after exposure to the SMF^[51].

For the I phase (**Figure 13A**), the sample at heating demonstrated spectral lines of protons in all three chemical groups of the ethylammonium cation and also a signal from water at ~ 4.7 ppm. In particular at lower temperatures, the contribution of the water NMR signal in the spectra of the I phase is much larger than the real fraction of water protons in the sample, because of the much longer NMR relaxation times of H_2O protons in comparison with protons of EAN and also because of an increase of the ^1H NMR signal at lower temperatures (Curie's law^[55]). Heating the sample up to 270 K did not significantly change the spectral form apart from minor changes in chemical shifts for NH_3^+ protons (from *ca.* 7.5 to 7.6 ppm) and for H_2O protons (from *ca.* 4.9 to 4.7 ppm) in the temperature interval from 256 to 266 K, respectively. In the temperature range of 270 – 285 K, spectral line intensities of ethylammonium progressively increased, while the contribution of the water signal decreased. Finally, the water signal almost disappeared at 293 K.

For the I_{MF} phase (see **Figure 13B**), the sample at heating in the range of 256-288 K showed only very weak spectral lines. This means that at these temperatures EAN was almost completely “frozen” without any significant motion of ions. In solids both the dipole-dipole interaction between protons and the ^1H chemical shift anisotropy, which are 2nd rank interactions with a strong orientation dependence, have dramatically broadened ^1H NMR resonance lines. The ^1H NMR spectral lines appeared at $T > 289$ K and the spectral shape was maintained at higher temperatures, demonstrating that EAN in this sample sharply and completely melted at 289 K. No signal from water was observed in ^1H NMR spectra for the I_{MF} phase. This may occur if water protons are under conditions of “fast exchange” with protons of $-\text{NH}_3$ groups of EAN^[39]. Usually, an exchange of protons of two chemical groups that differ in chemical shift leads to averaging of the chemical shifts and producing a line in the NMR spectrum with an intermediate value of chemical shift. Because $-\text{NH}_3$ protons in our system are in excess, the exchange can lead to disappearance of the NMR spectra line characteristic of bulk water for the I_{MF} phase. This explanation also suggests that water protons are under conditions of “slow exchange” in the I phase. Thus, $I \rightarrow I_{MF}$ transformation leads to a change of the dynamic state of water protons in the studied system from “slow exchange” to “fast exchange”. An alternative explanation of the disappearance of the water signal in the NMR spectrum of the I_{MF} phase is the increase of NMR relaxation rate of the water protons, i.e., T_2 decreased significantly in the I_{MF} phase and became so short that water protons did not contribute to the ^1H NMR echo signal. Such short ^1H NMR relaxation of water protons may be because water is actually expelled from EAN to the glass surfaces. It is known that adsorbed water possesses “solid-like” properties^[56] and, therefore, does not contribute to the ^1H NMR echo signal of a highly mobile liquid phase. In order to reveal the mechanism underlying this effect, we performed an additional experiment. The ^1H NMR line, corresponding to $-\text{NH}_3$ protons (~ 7.8 ppm), were pre-saturated using Bruker’s built-in NMR pulse sequences. It is known that pre-saturation leads to a decrease of the chemical exchange effect in the NMR spectrum^[57]. Therefore, a water proton signal should appear in the NMR spectrum in the case of proton exchange between H_2O and $-\text{NH}_3$ groups. Two NMR pulse sequences were used: Pre-saturation and Watergate 3-9-19 supersaturation. Both sequences gave similar results^[51]. The resonance line of $-\text{NH}_3$ protons at 7.8 ppm almost vanished, however no resonance line corresponding to water protons appears in the spectrum. This means that the “fast-exchange” mechanism does not take place in the system. Therefore, the other hypothesis, in which water is expelled from EAN and adsorbed on the glass plates, remains the most plausible explanation for the disappearance of the H_2O resonance line in the spectrum of EAN confined between polar glass plates.

Therefore, it can be concluded that the melting behaviour of the I and I_{MF} phases is significantly different. I phase melting proceeded in a rather broad temperature range, while in the I_{MF} phase complete melting occurred in a temperature range of only *ca.* 1 K. Additionally, the I_{MF} phase did not show any residual water NMR signal, most probably because water is expelled from the mixture with EAN and adsorbed on the polar glass surface.

Several additional experiments were performed to elucidate the properties of I_{MF} and I phases of EAN confined between glass plates^[51]. The sample after long-term exposure to the magnetic field in the NMR spectrometer (I_{MF} phase) was placed in a freezer at 193 K (-80°C) and kept there for twelve days. Afterwards, the sample was placed back in the NMR spectrometer at 293 K. Diffusion of EAN was then measured after the sample has completely thawed and the system reached a new thermal equilibrium. The measurement showed that the diffusion coefficient of EAN was equal to D_{MF} , thereby demonstrating that the transformation of $I_{MF} \rightarrow I$ was stopped in the frozen state of EAN. The sample in I_{MF} phase obtained for the orientation of the glass plates normal to the direction of the SMF was turned 90 degrees, so the plates became oriented along the magnetic field. Measurements demonstrated

that this manipulation did not affect the measured diffusion coefficient. The same happened when the orientation of the sample was changed from “parallel” to “normal” relative to the SMF. This experiment additionally demonstrated the isotropy of the I_{MF} phase.

Residual water, which is usually present in highly hygroscopic protic ILs, such as EAN and PAN, could obviously modify properties of the studied system. EAN/H₂O and bulk mixtures of some other protic ILs with water have been thoroughly studied^[52,58-62]. Molecular dynamics simulations suggested that at low concentrations of water in EAN a local sponge-like structure specific to this neat IL is not significantly altered by water molecules^[52,61]. Instead, water accommodates itself in the network of hydrogen bonds of the IL^[61] and leads to “swelling” of the polar regions in the bulk IL^[52]. According to data reported in^[51] for the sample of layers of EAN confined between polar glass plates and exposed to the external magnetic field, water is expelled from the IL and most probably is adsorbed on the polar glass surfaces.

3.6. Kinetics of phase transformations

Watching changes of NMR relaxation and diffusivities of cations of ILs with nitrate anion confined in layers between glass plates, we suggested that the processes occurring in the layers in the magnetic field can be related to a phase transformation. The change in the phase characteristics over time occurring at constant temperature has been analyzed by a heuristic Avrami equation^[63-66] (also known as a Johnson-Mehl-Avrami-Kolmogorov (JMAK) equation). This equation describes processes of the autocatalytic type, for example, a phase transformation occurring by a nucleation mechanism. The equation can specifically describe the kinetics of crystallization or other changes of phases in a material. The degree of phase transformation (fraction of a growing phase) is described as follows^[63]:

$$Y(t) = 1 - \exp(-Kt^n), \quad (6)$$

where K is a reaction rate constant, and the exponent n is a constant related to nucleation and growth. In our experiments, the parameter characterizing the phases is the diffusion coefficient. Therefore, the degree of phase transformation (fraction of phase I_{MF} formed in ILs between polar glass plates under the influence of the magnetic field) can be calculated as in Eq. (7):

$$Y(t) = (D_{init} - D(t))/(D_{init} - D_{fin}). \quad (7)$$

The calculated $Y(t)$ for the kinetics of transformation of EAN and PAN^[51] are shown in **Figure 14**. Dependences, $Y(t)$, were fitted by Eq.(6) using the least square method (**Figure 15**). Avrami parameters K and n used for the fittings are also shown in **Figure 15**.

For both EAN and PAN, the Avrami exponent n is close to 1. Originally, n was held to have an integer value between 1 and 4, which reflected the nature of the transformation^[63]. There were simulations to relate dimensionality and mechanism of crystallization with the observed Avrami exponent n . In earlier work of Cahn, $n = 1$ was related to a case of site saturation at nucleation on a surface^[67]. It has been shown^[68] that homogeneous as well as heterogeneous nucleation in the surface-independent and diffusion-independent deposition rates give $n \sim 1$ in a 3-dimensional system. This suggests the formation of a primary nucleus of a new phase spontaneously or on heterogeneous nucleation agents in the beginning of the process and further growth of the new phase by deposition of molecules from the original phase on the nucleus surface. The rate constant K is influenced by a ratio of interfacial to thermal energy. K is higher for PAN in comparison with EAN, because its thermal energy per mass of the PA cation is lower.

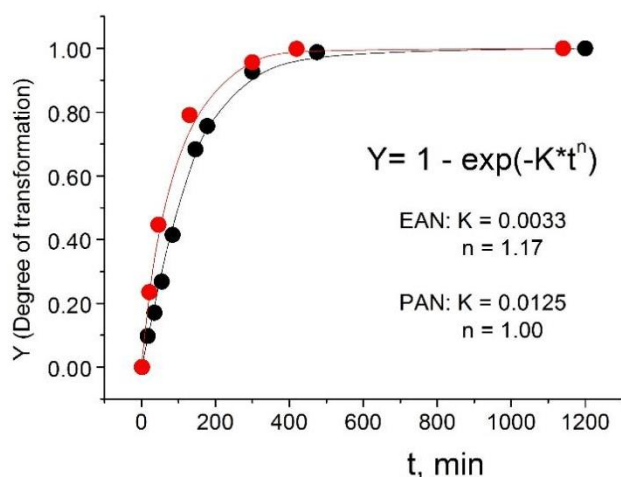


Figure 14. Degree of phase transformation (fraction of phase I_{MF}) as a function of time for EAN (black dots) and PAN (red dots) polar glass plates confined^[51]. Lines are best the Avrami equation fits with indicated values K and n .

Inspecting fits presented in **Figure 14**, one can conclude that the kinetics of transformations of phases in EAN and PAN exposed to a SMF can be described satisfactorily well by the Avrami equation using parameters characteristic for autocatalytic processes, which often are controlled by spontaneous nucleation. Kinetics of the phase transformation was analyzed also for the EAN-water system^[49]. It was shown that the kinetics of transformation fit well with the Avrami equation. The Avrami exponent n remains close to 1, which suggests that there is no change in the geometry of the growing phase, while the rate parameter K decreases with increased water up to 6.2 mol.% and increases again for a sample containing 12.4 mol.% water.

The kinetics of phase transitions of confined EAN and PAN fits well with Avrami phase transition theory. This demonstrates that the process is very likely autocatalytic and proceeds through a nucleation mechanism. The obtained value of the Avrami equation exponent n is close to 1, which can be described by homogeneous or heterogeneous nucleation in the surface-independent and diffusion-independent deposition rates in a 3D system.

Temperature measurements of solidification and melting behaviours showed a difference in phase transition temperatures, intervals of the phase transition temperatures and completeness of these transitions for confined phases of EAN formed before and after exposure in the magnetic field. An unexpected result was obtained that concerns the state of residual water under transformation of confined EAN under exposure to a magnetic field.

3.7. Reversibility of the $I \rightarrow IMF$ transformation

Dynamics of EAN reversibly recovered after removing the sample from the magnetic field. We have performed additional experiments with EAN confined between borosilicate glass plates to follow the kinetics of recovery from exposure to a magnetic field^[47]. The parameter measured was the diffusion coefficient of the EA cation. Experiments were performed at 293 K twice and with a different time sequence for confidence of the reproducibility of the effect. Before each experiment, the sample was kept outside of the magnetic field of the NMR spectrometer for at least one week. Later, the sample was placed in the diffusion probe of the NMR spectrometer (9.4 T). Enhanced diffusivity of the EA cation was registered in the beginning as well as a continuous decrease with time as described earlier. In the first experiment, the process of the diffusion coefficient decrease was followed almost to completion (~250 min), while in the second experiment, only to half completion (~100 min). Later, the sample was removed from the spectrometer. To trace changes of diffusivity during the process of recovery, the sample was kept outside the magnet and placed in the NMR spectrometer only for the few minutes required for a single measurement. We believe that the limited duration

of sample placement in the magnetic field (*ca.* 2-3 minutes) did not significantly distort the rather slow process of inverse phase transformation in confined EAN with a characteristic time constant of *ca.* 500 min.

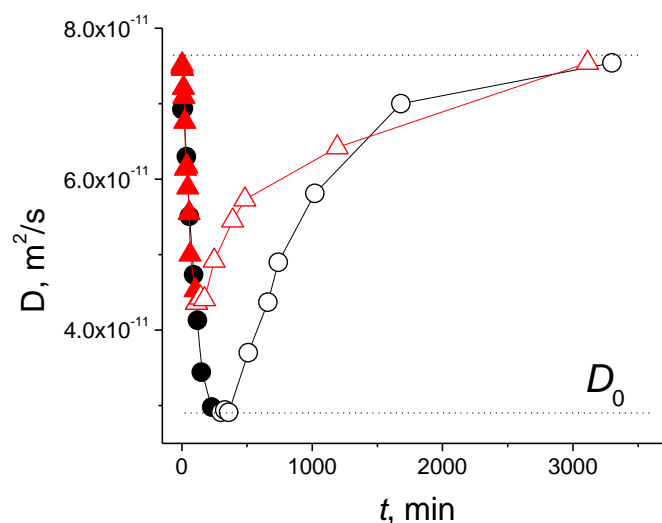


Figure 15. EA cations diffusion coefficients of EAN confined at borosilicate glass plates. D was measured along the plates, $t_d = 3$ ms. D_0 is the diffusion coefficient of EA in bulk EAN. Solid symbols – sample in the magnetic field 9.4 T, open symbols - after removal of the sample from the magnetic field^[47].

As seen from **Figure 15**, the process of recovery started just after removing the sample from the strong magnetic field, without a lag. Recovery curves demonstrate typical saturated behaviour. At the end of the process, D reaches the value that was measured at $t = 0$. The kinetics of the reverse phase transformation is well-described by the Avrami formula. The Avrami exponent n is close to 1, the same as was observed for direct transformation^[51], corresponds to homogeneous as well as heterogeneous nucleation in the surface-independent, and diffusion-independent deposition rates give $n \sim 1$ in a 3-dimensional system^[68]. Based on the Avrami analysis, we can suggest that mechanisms of reverse phase transformations are the same as the mechanism of direct transformation.

3.8. Rotating magnetic field

An effect of the SMF of the NMR spectrometer on the rotated anisotropic sample containing EAN layers confined between glass plates has been investigated^[50]. We studied the effects of rotation of the sample axis directed along plates relative to two axes: along and normal to the SMF B_0 of the NMR spectrometer (**Figure 16**).

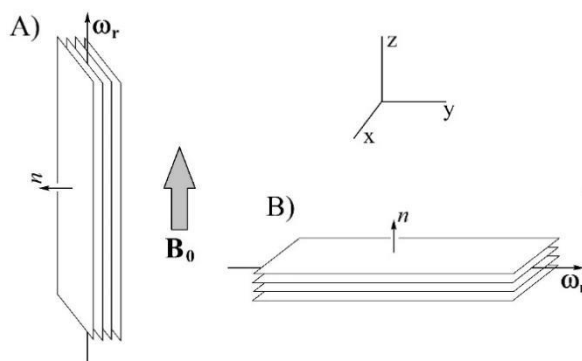


Figure 16. The scheme of the experiment with sample rotation relative to the SMF of the NMR spectrometer, B_0 ^[50]. ω_r is the axis of rotation of the sample. n is the direction normal to the sample.

In the first arrangement (**Figure 16A**), the sample was connected to the standard 5-mm NMR tube spinner. In this case, the sample was rotated around the z axis, parallel to the main SMF B_0 . The angle between n and the axis of rotation (90 degrees) did not change during rotation. The rate of rotation was ~ 20 Hz. In the second arrangement, an NMR solenoid ^1H insert was used to macroscopically align the plates (**Figure 16B**). In this case, the sample was rotated around the y-axis directed perpendicular to the direction of the main SMF B_0 . The rate of rotation was $1/3 \text{ min}^{-1}$ ($\sim 5.6 \cdot 10^{-3}$ Hz). To perform the NMR diffusion measurement, the rotation was stopped for both arrangements (A) and (B) and, in the case of (B); the sample was turned with n perpendicular to B_0 . So, mechanical collisions of EAN with the glass plates did not influence the values obtained for the diffusion coefficients, as was shown previously^[12].

Experiments showed that for arrangement (A) the diffusion coefficient decreases with time just after placement in the magnetic field at the same rate as for a static sample from D_I to D_{MF} . After the diffusivity has reached D_{MF} , the diffusivity does not change anymore until the sample is removed from the field. Thus, the effect of rotating the sample in the magnetic field around the axis parallel to B_0 is like that obtained previously for the static sample. In the case of arrangement (B), rotation of the sample for 18 hours after sample placement in the magnetic field does not affect the diffusion coefficient, which remains nearly equal to D_I for the duration of the experiment. However, after the rotation is stopped, D starts to decrease in the same manner as occurs with the static sample and with the rotating sample in the case of (A) (curve 4, open triangles), and finally reaches D_{MF} . Therefore, rotation of the EAN layers around the axis normal to B_0 stops the effect of a SMF: diffusivity of confined EAN does not change under the influence of a magnetic field under the latter conditions.

Characteristic time constants for transformations of dynamic phases of EAN placed between glass plates are on the order of a few hours. For example, the diffusivity decreases by a factor of two over approximately 70 minutes^[12]. For both arrangements used, (A) and (B), rotation of the sample occurs at different rates, ~ 20 Hz and $\sim 5.6 \cdot 10^{-3}$ Hz, but revolution times in both cases are much less than the time-scale of the EAN $I \rightarrow I_{MF}$ and $I_{MF} \rightarrow I$ phase transformations. Formations occurring in the I and I_{MF} phases of the confined EAN originate from EAN interacting with the polar surface of glass plates. Therefore, one of the possible mechanisms leading to the observed effects of sample rotation is the change in orientation of the surface layers of EAN interacting with Si-O-H groups near the glass plates, which contributes insignificantly to the NMR signal, but is nevertheless present^[3,15]. For the sample rotating around the axis directed along the magnetic field (A), the orientation of the surface layer does not change and the sample rotation does not influence the kinetics of the decrease in D , which remains typical for a stationary sample. However, for the sample under arrangement (B), rotation leads to a periodic change in the orientation of the surface layer. Because the interaction of EAN with the surface of the glass plates is responsible for the formation of the I and I_{MF} phases of EAN, the changing orientation of the surface layer of EAN relative to B_0 appears to be a leading factor resulting in preservation of the I phase. The surface layer of EAN may include up to seven molecular layers with a spatial range up to three nm^[3]. Subsequent interaction of the surface layer of EAN with other, more distant regions of the IL (\sim four μm), not directly interacting with the glass surface, occurs on a slower time scale and leads to modification of the H-bonding network of all the EAN confined between glass plates^[40]. It is known that EAN can form clusters with different structures of the H-bonding network^[69]. It is possible that the external influence can change the structure. We do not know how these proceed in our particular case. Additional simulations are necessary to elucidate how the interactions of EAN with the glass surface and the magnetic field alter the hydrogen-bonding network.

Variation of B_0 , ΔB , has been estimated by considering the variation of the ^1H NMR chemical shift $\Delta\delta$ at rotation of the sample from 0 to 90 degrees, using equations^[39]:

$$\Delta\omega = \Delta\delta \cdot \omega_0 \quad (8) \quad \text{and} \quad \Delta B = \Delta\omega / \gamma. \quad (9)$$

For $\Delta\delta \sim 4$ ppm, the estimation showed that $\Delta B \sim 4.0 \cdot 10^{-5}$ T. This is comparable to the width of the EAN ^1H NMR spectrum ($\sim 5.4 \cdot 10^{-5}$ T). Therefore, alteration of the magnetic field during the sample rotation may also prevent $I \rightarrow I_{\text{MF}}$ transformation or can cause $I_{\text{MF}} \rightarrow I$ transformation for the sample in arrangement (B). In this case, the H-bonding network should be involved in the transformation.

3.9. Ordering of ions in EAN confined between micrometer-spaced glass plates

Anisotropy of reorientational motion of molecules can be probed by ^2H NMR spectroscopy using deuterium-enriched samples^[70]. For a given C-D moiety, the quadrupolar splitting in the ^2H NMR spectrum depends on the angle between the C-D bond and the applied SMF. To check the anisotropy of the orientation of ethylammonium cations, a sample of EAN was synthesized which was selectively deuterated at CD_3 - and CD_2 - positions (~ 98 atom% of ^2H). This sample (EAN- D_5) was admixed into EAN with a natural abundance of ^2H and used to prepare a sample with EAN confined between glass plates. ^2H NMR spectra were obtained with the NMR Bruker spectrometer at a resonance frequency of 62.43 MHz for ^2H using the quadrupole-echo pulse sequence^[12]. ^2H NMR spectra of the sample are shown in Figure 17. There is no detectable quadrupolar splitting in the spectra. Therefore, there are no proof of the preferential ordering of CD_3 - and CD_2 - groups in the sample.

Because the nitrate anion of EAN does not contain protons, its ordering cannot be studied by ^2H NMR. However, ^{15}N and ^{17}O NMR are potentially informative for this purpose, especially ^{15}N NMR spectroscopy, which is extremely sensitive to the orientation of the spin orientation in a SMF^[39,71,72]. Because of the low natural abundance of ^{15}N and ^{17}O isotopes, a special isotopically enriched EAN ($^{15}\text{N},^{17}\text{O}$ -EAN) was synthesized with degrees of enrichment 38% for ^{17}O and 98% for ^{15}N ^[73]. Measurements were performed using NMR solenoid ^{15}N and ^{17}O inserts to macroscopically align the sample stack at different angles with respect to the direction of the magnetic field^[73].

The ^{15}N NMR spectrum of bulk $^{15}\text{N},^{17}\text{O}$ -EAN shows a symmetric line with a chemical shift of 374 ppm and linewidth of 0.04 ppm. The ^{15}N spectra of $^{15}\text{N},^{17}\text{O}$ -EAN confined between glass plates show broad lines with chemical shifts and the form of the spectra depends on the orientation of the sample (Figure 18)^[73]. As is seen from the figure, for the sample orientation with normal perpendicular to the induction of the magnetic field, a sharp signal is displaced upfield (right) relative to the bulk EAN signal, and a shoulder is observed on the side of the higher chemical shifts the down field against the sharp peak (**Figure 18C**).

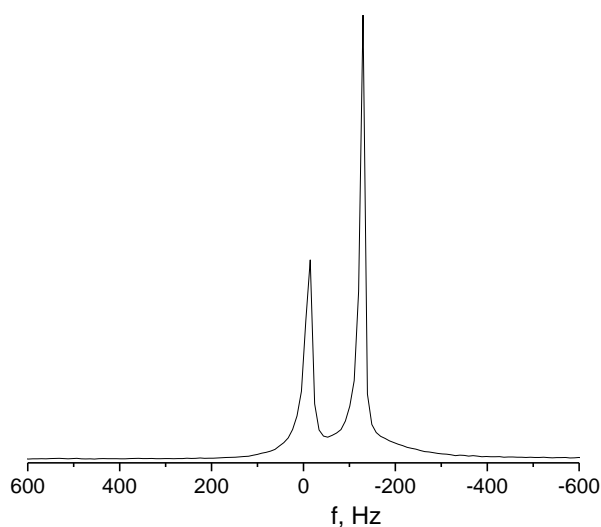


Figure 17. 62.43 MHz ^2H NMR spectra of 20 wt% of EAN- D_5 sample glass plates confined obtained by Solid-Echo sequence. $T = 293$ K. Sample normal was oriented at 90° to \mathbf{B}_0 .

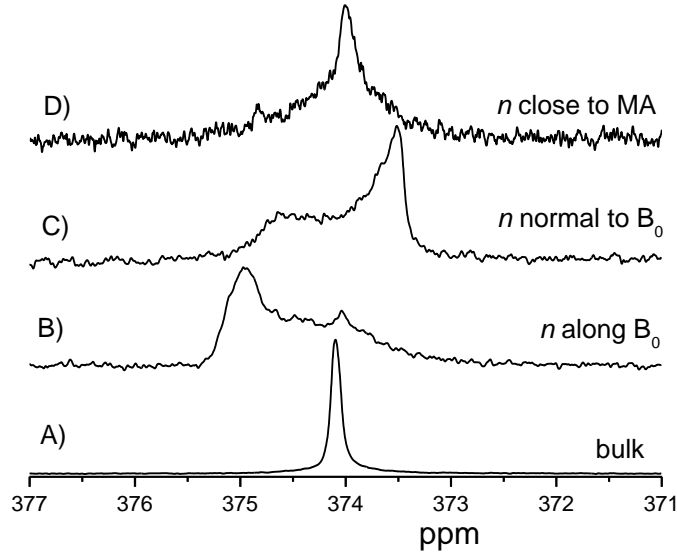


Figure 18. ^{15}N NMR spectra of $^{15}\text{N},^{17}\text{O}$ -EAN in bulk and glass plates confined after 20 h of exposure in the SMF.

For the sample orientation normal along the induction of the magnetic field, a sharp signal is displaced downfield relative to the bulk EAN signal (left), and a “shoulder” is observed on the side of the lower chemical shifts the up field against the sharp peak (**Figure 18B**). For the sample orientation close to 54.7° (at the “magic angle”^[39]), the chemical shift is close to that of the bulk sample (**Figure 18D**). Extended exposure of the sample to the magnetic field of the NMR spectrometer leads to a slow and continuous change in its ^{15}N NMR spectrum^[73]. It is known that the nuclear spin interaction with the SMF and motional averaging is described by secular Hamiltonian^[39]:

$$\hat{H}_j^{CS} \cong -\gamma_j \overline{\delta_{zz}^j(\Theta)} \mathbf{B}_0 \hat{I}_{jz}, \quad (10)$$

where the term δ_{zz}^j depends on the molecular orientation Θ and the chemical shift principal values. Because the two principal axes of symmetry of nitrate anion are equal, its structure is well represented by a uniaxial chemical shift tensor with the axis directed normally to the plate of the anion. The upfield ^{15}N chemical shift corresponds to the orientation at 0° to \mathbf{B}_0 (z-axis), while the downfield ^{15}N chemical shift corresponds to the 90° orientation (x and y axes).

A powder pattern for chemical shift anisotropy (CSA) of ^{15}N is a superposition of many sharp peaks with different frequencies, generally resulting in a sharp, nonsymmetric ^{15}N spectrum^[39,71]. Complete isotropic motional averaging characteristic for a liquid ^{15}N spectrum in liquids gives a narrow line, which is observed for bulk $^{15}\text{N},^{17}\text{O}$ -EAN. For the confined water-free EAN layers, broad lines of the spectra (**Figure 19B-19D**) are also conditioned by noncomplete motional averaging of the chemical shift. Additionally, orientation dependencies of the chemical shifts and form of the spectra are typical for anisotropy of the rotational motion^[39]. The orientation dependence of the ^{15}N spectrum demonstrates that for the case “ n along \mathbf{B}_0 ” (**Figure 18B**) the principal axis of the nitrate anion is preferentially oriented at 90° to \mathbf{B}_0 , while for “ n normal to \mathbf{B}_0 ” (**Figure 18C**) the principal axis of the nitrate anion is preferentially oriented at along \mathbf{B}_0 . Therefore, the principal axes of the nitrate anions are preferentially oriented perpendicular to the normal of the glass plates, n . Previously, a number of solvation layers of EAN were observed on a smooth silica surface^[3] extending up to 4 nm from the surface. It was found that the typical self-assembling structure formed near the surface consists of alternating layers of cations and anions with a preferential orientation of ions relative to the surface. For our sample containing EAN layers confined between glasses separated by $\sim 4 \mu\text{m}$, the contribution of surface layers with a thickness of 4 nm is only 0.1 %. Therefore, our ^{15}N NMR results demonstrate the ordering of the nitrate anion

occurring not or not only in thin surface layers but in the whole volume of the sample. Therefore, the nitrate anion is in an ordered state.

The distinct two-component form of the ^{15}N spectra of the confined water-free EAN, particularly just after the placement in the magnetic field means that alongside the one preferential orientation of the nitrate anion (normal to the plates), there are also another and even less ordered orientations of the anion principal axis relative to the glass plates. The last leads to the appearance of the broader ^{15}N spectrum component. Taking this into account, the change of the ^{15}N spectrum form at exposure to a SMF corresponds to “enhancing” the orientation of the anion normal perpendicular to the glass plates and decreasing other orientations.

It is known that the orientation of rotating spins at the “magic angle” effectively averages their dipolar coupling as well as the chemical shift anisotropy^[39]. In our case, orientation of the sample at the angle close to the “magic angle” (**Figure 18D**) leads to narrowing of the ^{15}N spectrum line. At the same time, the broad background signal remains non-averaged. This might be due to the imperfect mutual orientations of spins and the relatively weak dipole-dipole coupling of ^{15}N nuclei, which are rather far apart from each other.

It is known that EAN has a three-dimensional hydrogen bond network like water^[74,75]. EAN is a highly polar ILs, and it can interact with silanol groups on the polar surface of silica^[24,76]. The interaction of nitrate anion with silanol groups leads to the ordering of the nitrate anion, which is close to the surface. Changes in intermolecular interactions and electronic perturbations caused by variations in hydrogen bonds were observed by NMR chemical shift^[40,77]. The nitrate anion ordering further leads to rearrangement (weakening) of the hydrogen bonding network which further leads to the enhancing in molecular mobility of ions. The effect of placement of EAN layers is stronger for transverse NMR relaxation of protons of $-\text{NH}_3$ groups (decrease by a factor of ~ 22) in comparison with protons of other groups (by a factor of ~ 6). It is now evident that this is a result of the electrostatic interaction of the positively charged $-\text{NH}_3$ group with the nitrate anion undergoing anisotropic rotation.

Ordering of ILs placed between micrometer-spaced solid surfaces was observed by other researchers^[25,26]. Therefore, our observation of the ordering of EAN is in agreement with these studies. Translational and local dynamics of EAN confined between micrometer-spaced layers out and in the SMF is typical for liquid-crystal systems was observed not only for EAN but also for other ILs with nitrate anions, such as propylammonium nitrate^[51], 1-ethyl-3-methyl-imidazolium nitrate^[47] and mixtures of EAN with LiNO_3 ^[66]. This fact allows us to propose that the ordering of the nitrate anions occurs in all these systems too. Therefore, there is a need for further study in this field.

4. Conclusions and future perspectives

Several ionic liquids containing nitrate anion and their mixtures with salt with the same anion, enclosed between micrometre-spaced plates containing silicon oxide, demonstrate unusual dynamics, which is different from that in bulk and in nano-confinement of these ILs. The dynamics of the ions also reversibly changes during exposure of the ILs to a static magnetic field. These phenomena were analysed and interpreted as a result of phase transformations occurring in the enclosed ILs. Conditions of the transformations were investigated by dynamic NMR methods, NMR-diffusometry and NMR-relaxometry. Diffusivities of cations and anions in bulk are different because of the formed bi-continuous phase structure of the system. In the case of the placement of the ionic liquid between glass plates, interaction of anions with silanol groups on the surface leads to modification of the hydrogen bonding network in the whole EAN layer through NO_3^- - $-\text{NH}_3$ interaction. This does not lead to the ordering of CH_3^- and CH_2^- groups of rather flexible ethylammonium cation that is evident from deuterium NMR spectroscopy. For the nitrate anion having a hard plate-like structure, ^{15}N NMR spectra demonstrate preferential orientation of the principal axis of the anion relative to the surface of the glass plates. Therefore, bulk isotropic EAN, when placed within a micrometer-spaced enclosure, forms an ordered phase, which is similar to a liquid crystal. This phase has properties typical

for liquid crystals: the changed local and translational dynamics and a slow transformation kinetics occurring under the action of an external magnetic field. These effects being observed for EAN enclosed in micrometer-spaced layers do not observe for the IL confined in nano-sized pores of porous glasses, probably because of limitation on the minimal size for the formation of the liquid-crystalline phase.

Formation of ordered phases by ionic liquids enclosed between barriers of different size and geometry have to be investigated in detail. Effects of cation and anion structure, composition and properties of solid surface would be studied. T_1 , T_2 NMR relaxation and diffusivity as well as solid-state NMR experiments on natural isotopic abundance and isotopically ^2H , ^{11}B , ^{15}N , ^{17}O ionic liquid samples is very helpful for this purpose, as well as other physicochemical methods such as FTIR, Raman spectroscopy, X-ray diffraction and some other.

Acknowledgments

Authors thank Scriptia Academic Editing for English correction and proofreading of this manuscript. A.F. and O.N.A. acknowledges the Swedish Foundation for Strategic Research (project EM16-0013) for financial support. G.O.I. performed NMR measurements at the expense of a subsidy allocated to the Kazan Federal University to fulfill the state assignment in the field of scientific activity FZSM-2023-0016.

Competing interests

The authors declare no competing interests.

References

1. Zhang Sh, Zhang J, Zhang Y, Deng Y. Nanoconfined ionic liquids. *Chem. Rev.* 2017; 117: 6755-6833.
2. Filippov A, Taher M, Shah FU, Glavatskih S, Antzutkin ON. The effect of the cation alkyl chain length on density and diffusion in dialkylpyrrolidinium bis(mandelato)borate ionic liquids. *Phys. Chem. Chem. Phys.* 2014; 16: 26798-26805.
3. Gebbie MA, Smith AM, Dobbs HA, Lee AA, Warr GG, Banquy X, Valtiner M, Rutland MW, Israelachvili JN, Perkin S, Atkin R. Long range electrostatic forces in ionic liquids. *Chem. Commun.* 2017; 53: 1214-1224.
4. Hayes R, Warr GG, Atkin R. Structure and nanostructure in ionic liquids. *Chem. Rev.* 2015; 115: 6357-6426.
5. Wang YL, Li B, Sarman S, Mocci F, Lu ZhY, Yuan J, Laaksonen A, Fayer MD. Microstructural and dynamical heterogeneities in ionic liquids. *Chem. Rev.* 2020; 120: 5798-5877.
6. Hayes R, Imberti S, Warr GG, Atkin R. Amphiphilicity determines nanostructure in protic ionic liquids. *Phys. Chem. Chem. Phys.* 2011; 13: 3237-3247.
7. Sloutskin E, Lynden-Bell RM, Balasubramanian S. The surface structure of ionic liquids: Comparing simulations with x-ray measurements. *J. Chem. Phys.* 2006; 125: 174715.
8. Gil PS, Jorgenson SJ, Riet AR, Lacks DJ. Relationship between molecular structure, interfacial structure, and dynamics of ionic liquids near neutral and charged surfaces. *J. Phys. Chem. C* 2018; 122: 27462-27468.
9. Lexow M, Maier F, Steinrück HP. Ultrathin ionic liquid films on metal surfaces: adsorption, growth, stability and exchange phenomena. *Adv. Phys. X* 2020; 5: 1761266.
10. Elbourne A, Voitchovsky K, Warr GG, Atkin R. Ion structure controls ionic liquid near-surface and interfacial nanostructure. *Chem. Sci.* 2015; 6: 527-536.
11. Singh MP, Singh RK, Chandra S. Ionic liquids confined in porous matrices: physicochemical properties and applications. *Progr. Mater. Sci.* 2014; 64: 73-120.
12. Filippov A, Gnezdilov OI, Hjalmarsson N, Antzutkin ON, Glavatskih S, Furó I, Rutland MW. Acceleration of diffusion in ethylammonium nitrate ionic liquid confined between parallel glass plates. *Phys. Chem. Chem. Phys.* 2017; 19: 25853-25858.
13. Seyedlar AO, Stapf S, Mattea C. Nuclear magnetic relaxation and diffusion study of the ionic liquids 1-ethyl- and 1-butyl-3-methylimidazolium bis(trifluoromethylsulfonyl) imide confined in porous glass. *Magn. Reson. Chem.* 2019; 57: 818-828.
14. Iacob C, Sangoro JR, Papadopoulos P, Schubert T, Naumov S, Valiullin R, Kärger J, Kremer F. Charge transport and diffusion of ionic liquids in nanoporous silica membranes. *Phys. Chem. Chem. Phys.* 2010; 12: 13798-13803.
15. Iacob C, Sangoro JR, Kipnusu WK, Valiullin R, Kärger J, Kremer F. Enhanced charge transport in nano-confined ionic liquids. *Soft Matter* 2012; 8: 289-293.
16. Filippov A, Azancheev N, Shah FU, Glavatskih S, Antzutkin ON. Self-diffusion of phosphonium bis(salicylato)borate ionic liquid in pores of Vycor porous glass. *Micropor. Mesopor. Mater.* 2016; 230: 128-134.
17. Otero-Mato JM, Montes-Campos H, Cabeza O, Gallego LJ, Varela LM. Nanoconfined ionic liquids: A computational study. *J. Molec. Liq.* 2020; 320: 114446.

18. Filippov A, Antzutkin ON. Magnetic field effects dynamics of ethylammonium nitrate ionic liquid confined between glass plates. *Phys. Chem. Chem. Phys.* 2018; 20: 6316-6320.
19. Filippov A, Gnezdilov OI, Antzutkin ON. Dynamics of ethylammonium nitrate near PTFE surface. *Magn. Reson. Imaging* 2022; 85: 102-107.
20. Aslyamov T, Khlyupin A, Pletneva V, Akhatov I. Detailed characterization of rough surfaces for silica materials. arXiv:1908.01604v1 [cond-mat.mtr] 5 Aug 2019.
21. Ori G, Villemot F, Viau L, Vioux A, Coasne B. Ionic liquid confined in silica nanopores: molecular dynamics in the isobaric-isothermal ensemble. *Molec. Phys.* 2014; 112: 1350-1361.
22. Lahrar EH, Deroche I, Ghimbeu CM, Simon P, Merlet C. Simulations of ionic liquids confined in surface-functionalized nanoporous carbons: implications for energy storage. *ACS Appl. Nano Mater.* 2021; 4: 4007-4015.
23. Stephens NM, Masching HP, Walid MKI, Petrich JW, Anderson JL, Smith EA. Temperature-dependent constrained diffusion of micro-confined alkylimidazolium chloride ionic liquids. *J. Phys. Chem. B* 2022; 126: 4324-4333.
24. Atkin R, Warr GG. Structure in confined room-temperature ionic liquids. *J. Phys. Chem. C* 2007; 111: 5162-5168.
25. Anaredy RS, Shaw SK. Long-range ordering of ionic liquid fluid films. *Langmuir* 2016; 32: 5147-5154.
26. Pung H, Okada-Junior CY, Simoes M. Thermotropic ionic crystals (TILCs): Tunable-by-design self-assembling and stimuli-sensible electrolytic materials platform for energy applications, COIL-9 – 9th International Congress on Ionic Liquids, 24-28 April 2023. Lyon, France. <https://www.coil-9.congress-scientifique.com/en/program/online-program/22>
27. Pinilla C, Del Popolo MG, Lynden-Bell RM, Kohanoff J. Structure and dynamics of a confined ionic liquid. Topics of relevance to dye-sensitized solar cells. *J. Phys. Chem. B* 2005; 109: 17922-17927.
28. Berrod Q, Ferdeghini F, Judenstein P, Genevaz N, Ramos R, Fournier A, Dijon J, Olliver J, Rols S, Yu D, Moled RA, Zanotti JM. Enhanced ionic liquid mobility induced by confinement in 1D CNT membranes. *Nanoscale* 2016; 8: 7845-7848.
29. Tasserit C, Koutsioubas A, Lairez D, Zalcer G, Clochard MC. Pink noise of ionic conductance through single artificial nanopores revisited. *Phys. Rev. Lett.* 2010; 105: 260602.
30. Greaves TL, Drummond C. Protic ionic liquids: properties and applications. *Chem. Rev.* 2008; 108: 206-237.
31. Walden P. Über die Moleculargröße und Elektrische Leitfähigkeit Einiger Geschmolzener Salze. *Bull. Acad. Imp. Sci. St Petersburg* 1914; 8: 405-422.
32. Belieres JP, Angell CA. Protic ionic liquids: Preparation, characterization, and proton free energy level representation. *J. Phys. Chem. B* 2007; 111: 4926-4937.
33. Garlitz JA, Summers CA, Flowers II RA, Borgstahl GEO. Ethylammonium nitrate: A protein crystallization reagent. *Acta Cryst. D* 1999; 55: 2037-2038.
34. Zhao C, Burrell GT, Torriero AAJ, Separovic F, Dunlop NF, MacFarlane DR, Bond AM. Electrochemistry of room temperature protic ionic liquids. *J. Phys. Chem. B* 2008; 113: 6923-6936.
35. Mohamed MS, Aboud FA, Shakir I. Molybdenum oxide nanowires based supercapacitors with enhanced capacitance and energy density in ethylammonium nitrate electrolyte. *J. Alloys Compounds* 2015; 650: 123-126.
36. Plechkova NV, Seddon KR. Applications of ionic liquids in the chemical industry. *Chem. Soc. Rev.* 2008; 37: 123-150.
37. Atkin R, Warr GG. Structure in confined room-temperature ionic liquids. *J. Phys. Chem. B* 2008; 112: 4164-4166.
38. Kennedy DF, Drummond CJ. Large aggregated ions found in some protic ionic liquids. *J. Phys. Chem. B* 2009; 113: 5990-5993.
39. Levitt M. Spin Dynamics. Basics of Nuclear Magnetic Resonance (2nd Ed). Wiley & Sons; 2008.
40. Gnezdilov OI, Antzutkin ON, Gimatdinov R, Filippov A. Temperature dependence of ¹H NMR chemical shifts and diffusivity of confined ethylammonium nitrate ionic liquid. *Magn. Reson. Imag.* 2020; 74: 84-89.
41. Hayamizu K, Tsuzuki S, Seki S, Umebayashi Y. Nuclear magnetic resonance studies on the rotational and translational motions of ionic liquids composed of 1-ethyl-3-methylimidazolium cation and bis(trifluoromethanesulfonyl)amide and bis(fluorosulfonyl)amide anions and their binary systems including lithium salts. *J. Chem. Phys.* 2011; 135: 084505-1–084505-11.
42. Filippov A, Alexandrov AS, Gimatdinov R, Shah FU. Unusual ion transport behaviour of ethylammonium nitrate mixed with lithium nitrate. *J. Mol. Liq.* 2021; 340: 116841.
43. Cohen MH, Turnbull D. Molecular transport in liquids and gases. *J. Chem. Phys.* 1959; 31: 1164-1169.
44. Janz GJ, James DW. Molten nitrates as electrolytes: Structure and physical properties. *Electrochim. Acta* 1962; 7: 427-434.
45. Filippov A, Antzutkin ON, Arkhipov VP, Gnezdilov OI. Diffusivity of ethylammonium nitrate protic ionic liquid confined in porous glasses. *J. Mol. Liq.* 2022; 356: 118998.
46. Linse P, Söderman O. The validity of the short-gradient-pulse approximation in NMR studies of restricted diffusion. Simulations of molecules diffusing between planes, in cylinders and spheres. *J. Magn. Reson. A* 1995; 116: 77-86.
47. Filippov A, Antzutkin ON, Gimatdinov R, Gnezdilov OI. Self-diffusion in ionic liquids with nitrate anion: effects of confinement between glass plates and static magnetic field. *J. Mol. Liq.* 2020; 312: 113404.
48. Filippov A, Gnezdilov OI, Luchkin AG, Antzutkin ON. Self-diffusion of ethylammonium nitrate ionic liquid confined between modified polar glasses. *J. Mol. Liq.* 2019; 284: 366-371.
49. Filippov A, Kurakin S, Gnezdilov OI, Antzutkin ON. Effect of magnetic field on diffusion of ethylammoniumnitrate – water mixtures confined between polar glass plates. *J. Mol. Liq.* 2019; 274: 45-51.

50. Filippov A, Gimatdinov R, Antzutkin ON, Kuzina NA, Gnezdilov OI. Effect of rotating magnetic field on diffusivity of ethylammonium nitrate ionic liquid confined between micrometer-spaced glass plates. *J. Mol. Liq.* 2021; 323: 115008.
51. Filippov A, Gnezdilov OI, Antzutkin ON. Static magnetic field alters properties of confined alkylammonium nitrate ionic liquids. *J. Mol. Liq.* 2018; 268: 49-54.
52. Hayes R, Imberti S, Warr GG, Atkin R. How water dissolves in protic ionic liquids. *Angew. Chem. Int. Ed.* 2012; 124: 7586-7589.
53. Fagerlund G. Determination of specific surface by the BET method. *Mat. Constr.* 1973; 6: 239-245.
54. Abe H, Nakama K, Hayashi R, Aono M, Takekiyo T, Yoshimura Y, Saihara K, Shimizu A. Electrochemical anomalies of protic ionic liquid – water systems: A case study using ethylammonium nitrate – water system. *J. Chem. Phys.* 2016; 475: 119-125.
55. Turov VV, Leboda R. Application of ¹H NMR spectroscopy method for determination of characteristics of thin layers of water adsorbed on the surface of dispersed and porous adsorbents. *Adv. Colloid Interface Sci.* 1999; 79: 173-211.
56. Overloop K, Van Gerven L. NMR relaxation in adsorbed water. *J. Magn. Res.* 1992; 100: 303-315.
57. Aguilar JA, Kenwright SJ. Robust NMR water signal suppression for demanding analytical applications. *Analyst* 2016; 141: 236-242.
58. Yoshizawa M, Xu W, Angell CA. Ionic liquids by proton transfer: Vapor pressure, conductivity, and the relevance of ΔpK_a from aqueous solutions. *J. Am. Chem. Soc.* 2003; 125: 15411-15419.
59. Zarrougui R, Dhahbi M, Lemordant D. Transport and Thermodynamic Properties of ethylammonium nitrate–water binary mixtures: Effect of temperature and composition. *J. Solution Chem.* 2015; 44: 686-702.
60. Huang Y, Wan Z, Yang Z, Ji Y, Li L, Yang D, Zhu M, Chen X. Concentration-dependent hydrogen bond behavior of ethylammonium nitrate protic ionic liquid–water mixtures explored by molecular dynamics simulations. *J. Chem. Eng. Data* 2017; 62: 2340-2349.
61. Docampo-Alvarez B, Gómez-González V, Méndez-Morales T, Carrete J, Rodriguez JR, Cabeza O, Gallego LJ, Varela LM. Mixtures of protic ionic liquids and molecular cosolvents: a molecular dynamics simulation. *J. Chem. Phys.* 2014; 140:214502.
62. Yaghini N, Nordstierna L, Martinelli A. Effect of water on the transport properties of protic and aprotic imidazolium ionic liquids – an analysis of self-diffusivity, conductivity, and proton exchange mechanism. *Phys. Chem. Chem. Phys.* 2014; 16: 9266-9275.
63. Avrami M. Kinetics of phase change. I general theory. *J. Chem. Phys.* 1939; 7: 1103-1112; Avrami M. Kinetics of phase change. II transformation—time relations for random distribution of nuclei. *J. Chem. Phys.* 1940; 8: 212-225.
64. Kolmogorov A. On the Statistical Theory of the Crystallization of Metals. *Bull. Acad. Sci. URSS (Cl. Sci. Math. Nat.)* 1937; 3: 355-359.
65. Johnson W, Mehl R. Reaction kinetics in processes of nucleation and growth. *Trans. Am. Inst. Min. Engin.* 1939; 135: 416-442.
66. Mehl R, Cahn R. in *Physical Metallurgy*. R. Cahn, P. Haasen (eds.), Vol. 1, North-Holland Physics Publishing. 1983.
67. Cahn JW. Transformation kinetics during continuous cooling. *Acta Metallurgica* 1956; 4: 572-575.
68. Yang J, McCoy J, Madras G. Distribution kinetics of polymer crystallization and the Avrami equation. *J. Chem. Phys.* 2005; 122: 064901.
69. Bodo E, Mangialardo S, Ramondo F, Ceccacci F, Postorino P. Unravelling the structure of protic ionic liquids with theoretical and experimental methods: Ethyl-, propyl- and butylammonium nitrate explored by Raman spectroscopy and DFT calculations. *J. Phys. Chem. B* 2012; 116: 13878-13888.
70. Spiess H. W. Deuteron NMR — a new tool for studying chain mobility and orientation in polymers. *Adv. Polym. Sci.* 1985; 66: 23-58.
71. Hou X, Kirkpatrick RJ, Yu P, Moore D, Kim Y. ¹⁵N NMR study of nitrate ion structure and dynamics in hydrotalcite-like compounds. *Amer. Mineralogist* 2000; 85: 173-180.
72. Wiedemann C, Fushman D, Bordusa F. ¹⁵N NMR studies provide insights into physico-chemical properties of room-temperature ionic liquids. *Phys. Chem. Chem. Phys.* 2021; 23: 12395-12407.
73. Filippov A, Antzutkin ON. State of anion in ethylammonium nitrate enclosed between micrometer-spaced glass plates as studied by ¹⁷O and ¹⁵N NMR. *Phys. Chem. Chem. Phys.* 2023; 25: 14538-14545.
74. Hunt PA, Ashworth CR, Matthews RP. Hydrogen bonding in ionic liquids. *Chem. Soc. Rev.* 2015; 44: 1257-1288.
75. Zentel T, Kühn O. Properties of hydrogen bonds in the protic ionic liquid ethylammonium nitrate. *Theor. Chem. Acc.* 2017; 136: 87.
76. Kralj S, Zidansek A, Lahajnar G, Zimer S, Blinc R. Phase behavior of liquid crystals confined to controlled porous glass studied by deuteron NMR. *Phys. Rev. E* 1998; 57: 3021.
77. Tang X, Xu Y, Zhu X, Lu Y. Changes in microstructure of two ammonium-based protic ionic liquids proved by in situ variable-temperature ¹H NMR spectroscopy: influence of anion. *Magn. Reson. Chem.* 2018; 56: 73-79.